

TESTING FOUR ELASTIC FINITE-DIFFERENCE SCHEMES FOR BEHAVIOR AT DISCONTINUITIES

BY JIŘÍ ZAHRADNÍK, PETER MOCZO,* AND FRANTIŠEK HRON

ABSTRACT

Three second-order and one fourth-order finite-difference schemes are theoretically and numerically investigated for their behavior at elastic discontinuities. One of them is extended with new formulas for a flat free surface. Two of the schemes are consistent with the stress-continuity condition for P - SV waves at discontinuities coinciding with horizontal (or vertical) grid lines; none of them is consistent at diagonal discontinuities. Despite these significant theoretical differences, the numerical results from all four schemes are very similar. Moreover, the results compare well with semianalytic solutions for three different models.

A practical conclusion is that the recent finite-difference schemes are by no means free from the accuracy problems at elastic discontinuities. Nevertheless, the schemes provide synthetic seismograms whose differences are well below the level normally introduced by structural and focal uncertainties.

INTRODUCTION

Finite-difference methods are one of the most powerful tools for numerical investigation of seismic waves in complex media. In this paper, we focus on the so-called *heterogeneous schemes*, in which the same formulas are used for all grid points except the boundaries of a computational region. These formulas represent a discrete form of the equations of motion for heterogeneous media. Boundary conditions at internal material discontinuities are not discretized. The discontinuities, if present, are taken into account by spatial variation of the material parameters (Lamé parameters and density). In most schemes, special formulas are employed at the free surface (Vidale and Clayton, 1986; Sochacki *et al.*, 1987; Levander, 1988). A few schemes use the same formulas literally everywhere, including the free surface. They account for the medium outside the free surface, appearing in the scheme, by setting its Lamé parameters and density to zero. This approach was recommended for SH waves by Boore (1972), and we call it the *vacuum formalism*. A heterogeneous scheme of Zahradník and Urban (1984) with the vacuum formalism was applied to SH waves at curved free surfaces, and a very good agreement with an independent method by Van den Berg (1987) was found for canyons. To the best of our knowledge, the vacuum formalism has not been used in finite-difference methods for P - SV waves with the exception of an attempt by Zahradník and Hron (1992). Spectral (Fourier) methods often use similar approaches, but their discussion is beyond the scope of this paper.

In most heterogeneous schemes, the material parameters are represented by their actual *local* values or by arithmetic averages from two neighboring grid points (Kelly *et al.*, 1976; Stephen, 1983; Bayliss *et al.*, 1986; Virieux, 1986; Levander, 1988; Sochacki *et al.*, 1991). No information about the detailed

* Permanent address: Geophysical Institute, Slovak Academy of Sciences, Dúbravská cesta, 842 28 Bratislava, Czechoslovakia.

variations between the grid points is taken into account. The accuracy problems are documented for heterogeneous schemes of this type. Kelly *et al.* (1976) assumed these problems to be connected with artificial transition zones. Virieux (1986) and Stephen (1983) claimed that the transition zone is not the problem, since the results did not change with grid refinements. Serious accuracy problems at solid-solid interfaces were found by Stephen (1983). He even reported instabilities for liquid-solid interfaces, which he overcame in a later paper by a special treatment of the material parameters (Stephen, 1988). The scheme by Virieux (1986) is stable for the liquid-solid interface, but a 20% amplitude discrepancy was found for Rayleigh waves in the simple Lamb's problem. Some problems at an internal discontinuity were also seen in Figure 9 of Daudt *et al.* (1989). The scheme of Kelly *et al.* (1976) was shown to be less accurate by Sochacki *et al.* (1991, Fig. 3). A great sensitivity of the heterogeneous schemes with respect to the particular approximations of the material parameters was also discussed by Kummer and Behle (1982) for polygonal boundaries (see, e.g., their Fig. 8). Fornberg (1987) outlined possible problems with the spatial sensitivity of the higher-order methods on relatively coarse grids, mainly when boundaries fall between mesh points.

In a few schemes, the actual variations between the grid points are approximated by certain integral averages, called *effective parameters* (Boore, 1972; Kummer and Behle, 1982; Zahradník, 1985; Kummer *et al.*, 1987; Zahradník and Hron, 1987; Moczo, 1989; Zahradník, 1990). With their help, for example, the distance from a discontinuity to a grid point can be accurately accounted for. Therefore, the latter schemes seem to be useful mainly on relatively coarse grids. In general, however, the schemes with effective parameters do not provide automatically the correct behavior at elastic discontinuities. On the other hand, some schemes without effective parameters (i.e., with the local parameters only) perform very well. As an example, the scheme by Levander (1988) was found to agree very well with the reflectivity method. Very likely, it was because no spatial derivatives of the material parameters occurred in the first-order equations of motion he used.

Most of the heterogeneous schemes are derived from the *differential* equations of motion. Others are derived from the *integrated* equations of motion, expressing the force balance of an elementary grid volume (Samarskii, 1977, Chap. 3, Sec. 2). The traction-continuity condition can also be included in the integral formulation (Sochacki *et al.*, 1991). However, when discretized, even the integral formulation can violate the traction continuity condition, mainly at discontinuities not coinciding with grid lines. On the other hand, some heterogeneous schemes derived from the differential equations can automatically satisfy the boundary conditions rather well. For example, Moczo (1989) demonstrated a very good agreement of such a scheme with the Aki-Larner discrete wave-number method for *SH* waves in basin-like structures. Bayliss *et al.* (1986), Levander (1988), and Stephen (1988) presented other encouraging examples of the agreement between independent solutions and the schemes based solely on the differential equations.

This short review demonstrates that the modern heterogeneous schemes represent a rather various class of different approaches. Hence, some classification with respect to their behavior at internal elastic discontinuities and free surfaces is desirable. Accordingly, the main objectives of this paper are formulated in the following way: (1) proposition of the method for a theoretical

evaluation whether a given scheme is consistent with the boundary conditions, or not; (2) application of such a method to the recent schemes, described by Kummer *et al.* (1987), Sochacki *et al.* (1991), and Zahradník and Hron (1992); (3) mutual comparison of the numerical results produced by all these schemes; and (4) comparison of their numerical results with those produced by some other independent methods (Alekseev and Mikhailenko, 1980; Bard and Bouchon, 1985; Kawase and Aki, 1989).

BOUNDARY BEHAVIOR OF THE SCHEMES: THEORY

In this section, we evaluate the boundary behavior of the schemes KBD (Kummer *et al.*, 1987), FD2 (Zahradník and Hron, 1987), and SGES (Sochacki *et al.*, 1991) briefly rederived and compared in Appendix 1. For this purpose, as in the standard analysis of the consistency of the finite-difference schemes for homogeneous media, we express discrete displacement values by means of their Taylor expansions in two spatial variables, substitute them into the schemes, and study their limit for $h \rightarrow 0$. In the case of heterogeneous schemes, such a procedure can be carried out even at a discontinuity, provided that the Taylor expansion is treated with care.

The SH Case

Boundary Conditions. The boundary conditions require the continuity of displacement and traction across the boundary. Since a single difference equation applies to each point on a discontinuity, the displacement continuity is automatically satisfied in any heterogeneous scheme. The continuity of the traction (y component) at a surface whose normal has x and z components n and m leads to

$$\mu v_x n + \mu v_z m = \mu' v'_x n + \mu' v'_z m, \quad (1)$$

with the denotation explained in Appendix 1. The parameters and derivatives with and without primes refer to their limiting values from both sides of the interface. Investigation of this condition at several different local shapes of the interface is considered next.

Horizontal (or Vertical) Discontinuity (Figs. 1a and 1b). As shown in Appendix 1, the KBD and FD2 schemes are identical for *SH*-wave propagation. Moreover, in case of a horizontal discontinuity, the material parameters make the SGES scheme identical with the KBD and FD2 too, according to equation (A11). Then, at a central point $(0, 0)$ of a grid stencil located on the discontinuity, all three *SH* schemes read

$$\begin{aligned} & 1/2(\mu + \mu')(v_{1,0} - 2v_{0,0} + v_{-1,0}) + \mu(v_{0,1} - v_{0,0}) + \mu'(v_{0,-1} - v_{0,0}) \\ & = 1/2(\rho + \rho')(h^2/k^2)(v_{new,0} - 2v_{0,0} - v_{old,0}), \end{aligned} \quad (2)$$

where v_{new} , v , and v_{old} relate to the time levels $M + 1$, M , and $M - 1$, respectively. After substituting the Taylor expansion up to the terms

proportional to h^2 , inclusively, and multiplying equation (2) by h , we get

$$h\{1/2(\mu + \mu')(v_{xx} + v'_{xx})/2 + 1/2\mu'v'_{zz} + 1/2\mu v_{zz} - 1/2(\rho + \rho')v_{tt}\} + O(h^2) + O(k^2h) + \mu v_z - \mu'v'_z = 0. \quad (3)$$

In the limit of $h \rightarrow 0$ we obtain the condition $\mu v_z - \mu'v'_z = 0$. It could also have been obtained directly from the first-order Taylor expansion. Since $n = 0$ and $m = 1$, this condition is equivalent to the required traction continuity (1). The same procedure for a vertical discontinuity ($n = 1, m = 0$) yields $\mu v_x - \mu'v'_x = 0$ that is again equivalent to (1).

The above result can be interpreted in the following way: When applied on the material discontinuity, the equation of motion yields (in sense of generalized functions) an additional body-force term. It is just this term that, after properly discretizing the equation of motion, can guarantee the traction continuity. The heterogeneous scheme resembles, in this respect, the seismic-source modeling by means of body-force equivalents: Instead of prescribing the displacement discontinuity at a fault plane, a body-force term is added to the equation of motion.

Diagonal Discontinuity (Fig. 1c). Both the KBD and FD2 schemes become identical once again. The material parameters of the SGES scheme need a deeper consideration, because the $a_{1,-1}$ and $a_{-1,1}$ values needed in equation (A11) are not clearly defined. If, however, the integration of the equations of motion is performed for this particular geometrical configuration analogously to Sochacki *et al.* (1991), it becomes evident that $a_{1,-1} = \mu'$, $a_{-1,1} = \mu$ are the appropriate values. These values also make the SGES scheme identical with the KBD and FD2 schemes for *SH* waves.

After repeating the procedure described above, retaining only the first-order Taylor terms, and performing the limit of $h \rightarrow 0$, we get

$$\mu v_x + \mu v_z - \mu'v'_x - \mu'v'_z = 0. \quad (4)$$

Realizing that $n = m$, we again arrive at the desired traction continuity (1) for all the three analyzed schemes.

The 90° Wedge (Fig. 1d). The Taylor expansion yields terms $uv'_z, \mu'v'_z$ that are difficult to interpret. If, however, we additionally assume $v_x = v'_x$ at the horizontal segment of the wedge, and $v_z = v'_z$ at the vertical one, the expansion provides (for $h \rightarrow 0$) exactly the same formula as for the *diagonal* discontinuity (equation 4). The same result takes place for the KBD, FD2, and SGES schemes. As both assumptions are correct independently in a locally planewave approximation at the horizontal and vertical boundaries, respectively, we could conclude that the 90° wedge is artificially transformed into a diagonal discontinuity, at which the traction continuity is satisfied. It is questionable, however, to what extent the locally plane wave approximation is acceptable in a small vicinity of the wedge.

Oblique (Nondiagonal) Discontinuity (Fig. 1e). Both the KBD and FD2 schemes work as if the *diagonal* discontinuity would have taken place. On the other

hand, a formal application of the SGES scheme with $a_{1,-1} = \mu$, $a_{-1,1} = \mu'$ yields

$$\mu v_x - \mu' v'_x = 0. \tag{5}$$

This means that the SGES scheme artificially transforms an arbitrary oblique nondiagonal discontinuity of Figure 1e (where the angle with respect to the vertical axis is less than $\pm 45^\circ$) into a *vertical* discontinuity. Similarly, for the angle less than $\pm 45^\circ$ with respect to the horizontal axis, the oblique discontinuity transforms into a *horizontal* one. The traction continuity at these artificially transformed surfaces is then satisfied.

Horizontal Discontinuity Not Coinciding with a Grid Line (Fig. 1f). We start with the KBD and FD2 schemes. No first-order Taylor terms are obtained from $(\mu v_x)_x$. From $(\mu v_z)_z$, according to (A4a), we get the term

$$\mu(v_{0,1} - v_{0,0}) - \mu_G(v_{0,0} - v_{0,-1}). \tag{6}$$

The difference $v_{0,0} - v_{0,-1}$ cannot be simply expressed by v_z , or v'_z . If we assume, however,

$$v_{0,0} - v_{0,-1} = h(\gamma v_z + [1 - \gamma]v'_z) \tag{7}$$

and compute effective parameter μ_G according to (A4b), we see that for $h \rightarrow 0$ we get $\mu v_z - \mu' v'_z = 0$, as required for a *horizontal* discontinuity *passing through point* (0, 0). We conclude that the KBD and FD2 schemes satisfy the traction continuity at the discontinuity artificially shifted to point (0, 0). The present example well illustrates the importance of geometric averaging (equation A4b). If, for example, one would use an arithmetic average for defining μ_G , instead of (A4b), the traction continuity will neither be satisfied at the artificially shifted discontinuity, nor the point (0, 0) will behave as being located in a homogeneous medium.

As far as the SGES scheme is concerned, the material parameter appearing with $(v_{0,0} - v_{0,-1})$ is μ' , according to (A11) and Figure 1f. As a result we get

$$\mu v_z - \mu'(\gamma v_z + [1 - \gamma]v'_z) = 0, \tag{8}$$

meaning that the traction continuity is neither satisfied at point (0, 0), nor does the point behave as one located in a homogeneous medium.

Vacuum Formalism. The preceding analysis can be completely repeated for $\mu' \rightarrow 0$, $\rho' \rightarrow 0$ (the vacuum). Note that the shear-wave velocity then becomes undefined. This, however, yields no problem, since the equation of motion does not operate with the velocity. In other words, the conclusions given above apply also to the free surfaces. The *SH* heterogeneous schemes KBD, FD2, and SGES can be applied up to the free surface inclusively, while the medium outside the surface is treated as vacuum. The traction-free conditions are satisfied under the same conditions as in the previous paragraphs, and no special free-surface formulas are needed for the *SH* case. We would have come to the same conclusion by proving that the *SH* scheme with the vacuum formalism is identical with the scheme expressing the symmetry condition (using central differences), which in turn is equivalent to the traction-free condition in the *SH* case.

The P-SV Case

Boundary Conditions. The requirement of the traction continuity (x and z components) can be written

$$\begin{aligned}
 &([\lambda + 2\mu]u_x + \lambda w_z)n + \mu(w_x + u_z)m \\
 &= ([\lambda' + 2\mu']u'_x + \lambda' w'_z)n + \mu'(w'_x + u'_z)m, \\
 &\mu(w_x + u_z)n + (\lambda u_x + [\lambda + 2\mu]w_z)m \\
 &= \mu'(w'_x + u'_z)n + (\lambda' u'_x + [\lambda' + 2\mu']w'_z)m.
 \end{aligned} \tag{9}$$

Horizontal (or Vertical) Discontinuity (Figs. 1a and b). A complete analysis is lengthy, but straightforward. We start with a horizontal discontinuity ($n = 0, m = 1$). For the *KBD scheme*, the first-order Taylor expansion and the limit of $h \rightarrow 0$ yield

$$\begin{aligned}
 &\mu 1/2(w_x + w'_x) + \mu u_z - \mu' 1/2(w_x + w'_x) - \mu' u'_z = 0, \\
 &\lambda 1/2(u_x + u'_x) + (\lambda + 2\mu)w_z - \lambda' 1/2(u_x + u'_x) - (\lambda' + 2\mu')w'_z = 0.
 \end{aligned} \tag{10}$$

This is obviously not equivalent to the boundary condition (9). If, however, we additionally assume $w_x = w'_x, u_x = u'_x$, which is true in a locally plane wave approximation at the flat boundary, then (10) transforms to the required condition (9). Quite similarly, the assumption of $w_z = w'_z$ and $u_z = u'_z$ guaran-

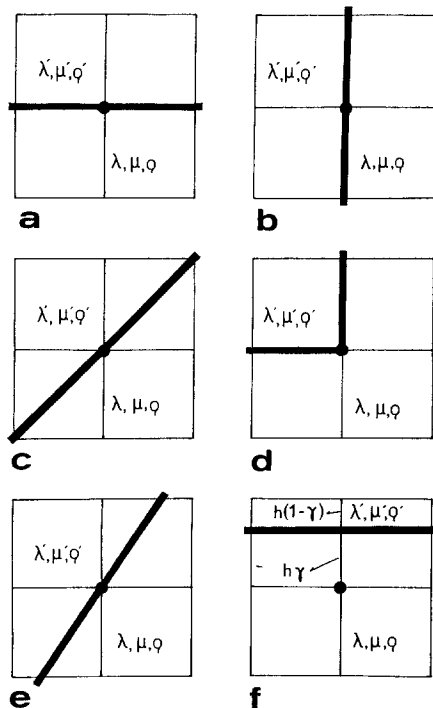


FIG. 1. Geometrical configurations of an elastic discontinuity (heavy line) with respect to grid lines. The finite-difference schemes are analyzed for their boundary behavior at the central point (full circle).

tees the stress continuity at the vertical discontinuity (equation 9 with $n = 1$, $m = 0$). As we see, unlike the *SH* case, an additional assumption is necessary. This assumption, however, is quite reasonable and acceptable. Another, more important difference with respect to the *SH* case appears when we try to use the KBD scheme in the vacuum formalism at a horizontal free surface for the *P-SV* case. The Taylor expansion then yields

$$\begin{aligned} 1/4\lambda w_x + 26/24\mu w_x + \mu u_z &= 0, \\ 1/4\mu u_x + 26/24\lambda u_x + (\lambda + 2\mu)w_z &= 0. \end{aligned} \quad (11)$$

What we need in accordance with (9) is

$$\begin{aligned} \mu w_x + \mu u_z &= 0, \\ \lambda u_x + (\lambda + 2\mu)w_z &= 0. \end{aligned} \quad (12)$$

Hence the boundary condition is strongly violated by terms $1/4\lambda w_x$ and $1/4\mu u_x$. (The difference due to the replacement of 1 by 26/24 is much less important.) Special formulas, extending the KBD scheme to the flat free surfaces and consistent with the required condition (12), are given in Appendix 2.

As the next step we analyze the *FD2 scheme* at a horizontal discontinuity, thereby getting

$$\begin{aligned} 1/2\mu w_x + \mu u_z - 1/2\mu' w'_x - \mu' u'_z &= 0, \\ 1/2\lambda u_x + (\lambda + 2\mu)w_z - 1/2\lambda' u'_x - (\lambda' + 2\mu')w'_z &= 0, \end{aligned} \quad (13)$$

Evidently, the traction continuity is *not* guaranteed by the *FD2 scheme*. It is violated by coefficients $1/2$ appearing (instead of 1) with w_x, w'_x, u_x, u'_x . The discrepancy, resulting from the incorrect boundary behavior of the present scheme, takes form of the additional false stresses, proportional to the horizontal derivatives of the displacement field. Exactly the same is true about the free surface. The fourth-order version *FD4* is analogous in this respect.

Finally, the *SGES scheme* is examined at a horizontal discontinuity. According to (A1a and b) and (A14), the only terms representing the difference with respect to the *FD2 scheme* are now only those coming from $(\mu w_x)_z, (\lambda u_x)_z$; i.e.

$$\begin{aligned} 1/4h^2\{(\mu - \mu')(w_{1,0} - w_{-1,0})\}, \\ 1/4h^2\{(\lambda - \lambda')(u_{1,0} - u_{-1,0})\}. \end{aligned} \quad (14)$$

The analogous terms, related to the derivatives $(\lambda w_x)_x, (\mu u_z)_x$, vanish in this particular geometrical configuration. The Taylor expansion of (14), multiplied by h , and the assumptions $w_x = w'_x, u_x = u'_x$ (the same as for the KBD scheme) yield a contribution from the additional terms (14) in the form of

$$\begin{aligned} 1/2(\mu - \mu')(w_x + w'_x)/2 &= 1/2\mu w_x - 1/2\mu' w'_x, \\ 1/2(\lambda - \lambda')(u_x + u'_x)/2 &= 1/2\lambda u_x - 1/2\lambda' u'_x. \end{aligned} \quad (15)$$

As it is seen from (13), the terms shown in (15) are those missing in the *FD2 scheme*. Therefore, after the terms (15) are added to (13), the traction continuity (9) is guaranteed in the complete *SGES scheme*. The same is also true about the

horizontal free surface treated by the vacuum formalism in the SGES scheme. At a vertical discontinuity (internal or free) the SGES scheme is boundary consistent upon the assumption of $u_z = u'_z$, $w_z = w'_z$.

Diagonal Discontinuity (Fig. 1c). None of the studied schemes is consistent with the traction continuity (9) in this case. The only assumption, which would yield (9) in the KBD scheme, is $w_z = w'_z$, $w_x = w'_x$ (when solved for u), and $u_z = u'_z$, $u_x = u'_x$ (when solved for w), respectively. Such assumptions are evidently not acceptable. The same applies to the SGES scheme if the parameters of the medium in (A12) are treated as required when integrating the equation of motion at this particular case:

$$\alpha_{-1,1} = \alpha, \quad \alpha_{1,-1} = \alpha', \quad \alpha_{-1,-1} = \alpha', \quad \alpha_{1,1} = \alpha. \quad (16)$$

Summary of the Theoretical Analysis

All the three studied schemes (KBD, FD2, and SGES) are equivalent for *SH* waves at horizontal (or vertical) discontinuities. The traction continuity is always guaranteed. Moreover, the vacuum formalism can be used at free surfaces of that type.

In the case of *P-SV* waves, the schemes differ from one another at horizontal (or vertical) discontinuities. Although the KBD scheme is derived from the differential equations of motion, its boundary behavior is theoretically as good as that of the SGES scheme, derived from the integrated equations. Even though the KBD and FD2 schemes are of the same order of accuracy and based on a similar approach, the KBD satisfies the boundary conditions, while FD2 does not.

A similar treatment of other geometrical configurations is more complicated and suggests that, in general, the accuracy problems might arise for the *P-SV* wave propagation in heterogeneous schemes on curved discontinuities. Even such a simple case like the diagonal discontinuity falls into this category.

BOUNDARY BEHAVIOR OF THE SCHEMES: NUMERICAL EXPERIMENTS

The preceding analysis does not provide a quantitative estimate of the boundary-introduced inaccuracies. This feature of the studied schemes is addressed by numerical experiments in this section.

Three models are investigated: a homogeneous halfspace (A), a sediment-filled valley (B), and a sedimentary basin (C). The model parameters are summarized in Table 1 and Figure 2. A constant density of $\rho = 1$ is assumed. The models are dimensionless, described by means of two reference quantities, T and L . Here

TABLE 1
PARAMETERS OF THE COMPUTATIONAL MODELS A, B, AND C

Model	$\frac{\alpha_{min}}{\beta_{min}}$	$\frac{\alpha_{max}}{\beta_{max}}$	$\frac{\beta_{max}}{\beta_{min}}$	$\frac{f_{max}}{f_0}$	$\frac{H}{L}$	$\frac{V}{L}$
A	2	2	1	2.5	10	10
B	2	$\sqrt{3}$	5	2.069	8	7.2
C	2	2	2.5	3.2	12.8	6.4

The *P*- and *S*-wave velocities = α and β (the minimum and maximum values); the predominant and maximum frequency of the excitation = f_0 and f_{max} ; the horizontal and vertical dimensions of the computational region = H, V ; the minimum shear wavelength = L . See also Figure 2.

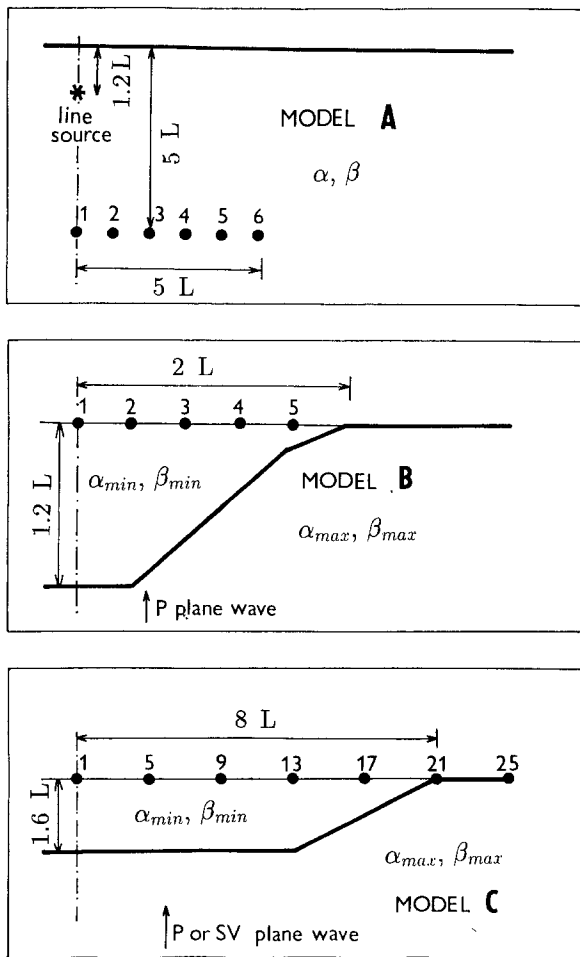


FIG. 2. Computational models A, B, C, for which four finite-difference schemes and three independent methods were compared. The plane of symmetry (antisymmetry) is represented by a dotted-dashed line; the discontinuities are shown in heavy lines. The receivers are marked by the full circles. The corresponding synthetics are given in Figures 3 to 6. For more details, see Table 1. Model B is taken from Bard and Bouchon (1985). Model C is equivalent to that of Kawase and Aki (1989), provided $f_0 = 0.5$ Hz, $T = 0.625$ sec, and $L = 625$ m.

$T = 1/f_{max}$ is an approximation of the minimum period, with f_{max} being defined in Table 1 and $L = \beta_{min} \cdot T$ being an approximation of the minimum shear wavelength.

Model A is excited by a line explosive source, the time function of which is

$$f(t) = \sin\{2\pi f_0 t\} \exp\{-4\pi^2 f_0^2 t^2 / 16\}, \quad f_0 = 1 \text{ Hz.} \quad (17)$$

The source is specified by means of the body-force equivalent of Aboudi (1971), applied to a grid square $2h$ by $2h$. Models B and C are excited by a vertically incident plane wave (P in models B and C and SV in model C); the algorithm of Alterman and Karal (1968) is used. The source wavelet in model B is given by

$$f(t) = \cos\{2\pi f_0 t\} \exp\{-4\pi^2 f_0^2 t^2 / 56.25\}, \quad f_0 = 2.41666 \text{ Hz,} \quad (18)$$

while that in model C is

$$f(t) = (2\pi^2 f_0^2 t^2 - 1) \exp\{-\pi^2 f_0^2 t^2\}, \quad f_0 = 0.5 \text{ Hz}. \quad (19)$$

All the three models are studied inside a rectangular computational region; see H and V in Table 1. The upper boundary is free (for details, see below). The left-hand boundary is symmetrical for w and antisymmetrical for u (vice versa in model C excited by the SV waves). The right-hand and the bottom boundaries are nonreflecting in the sense of Reynolds (1978) and Emerman and Stephen (1983), respectively. It should be mentioned that the Emerman-Stephen condition was originally also applied on the right-hand boundary, but later the Reynolds conditions were found better, mainly for the w components of model C and the SV incidence. Strictly speaking, we applied the Reynolds scalar formula independently to u and w components with the local velocities of P and S waves, respectively. Repeated computations for different sizes of the computational region (not shown here) were used for checking the performance of the non-reflecting boundaries.

Synthetic seismograms for models A, B, and C (Figs. 3 to 6) were computed by the three second-order finite-difference schemes (KBD, FD2, and SGES), which were theoretically compared in the preceding section. In addition, a fourth-order version of the FD2 scheme, denoted FD4, was also used. The spatial grid step h has been uniformly determined for models A, B, and C in such a way that $h = L/10$ has been used in all second-order schemes, and $h = L/5$ in the fourth-order scheme FD4. Significantly larger models would, of course, require finer grids. The time step k has been uniformly determined in all the second-

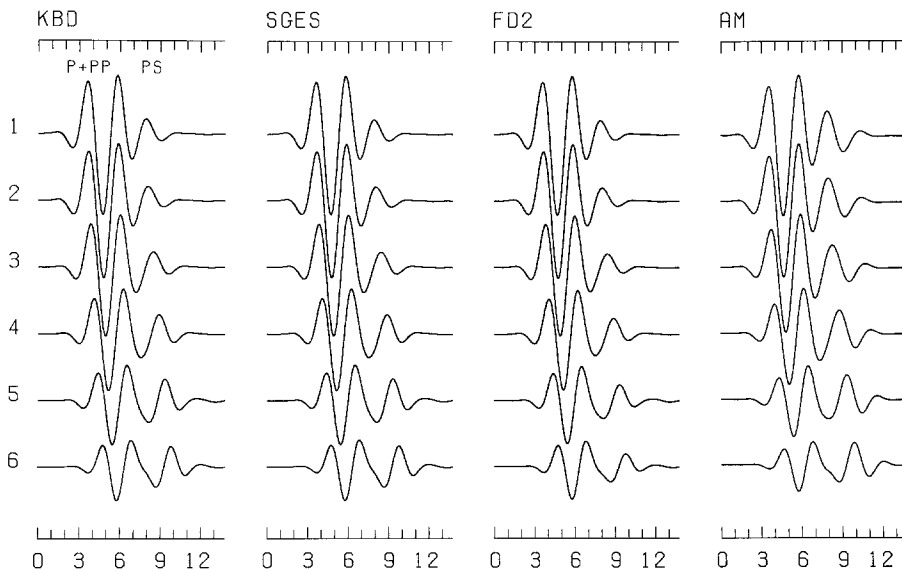


FIG. 3. Synthetic seismograms for a half-space model A, excited by an explosive line source. The horizontal axis is dimensionless (t/T). The synthetic traces by three second-order finite-difference schemes KBD, SGES, and FD2 are compared with those produced by an independent method of Alekseev and Mikhailenko (1980), AM. The seismograms by an economical fourth-order scheme FD4 are not shown separately since, in this case, they coincide within the width of line with those produced by FD2 scheme. The vertical component is presented.

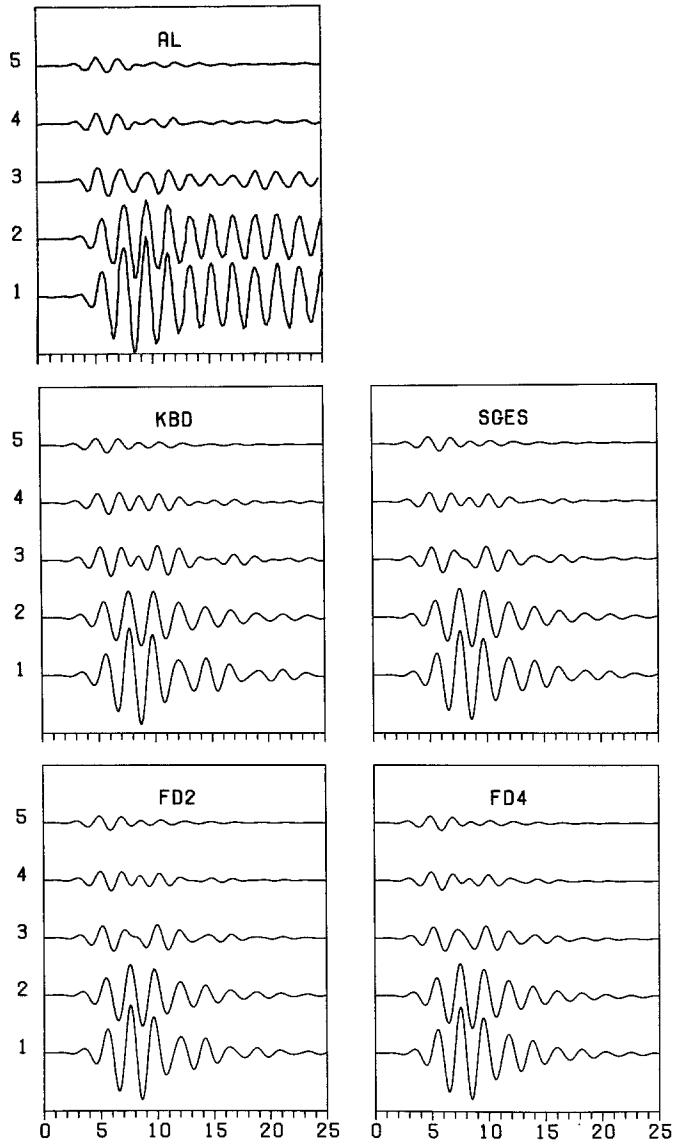


FIG. 4. Synthetic seismograms for a sediment-filled valley model B, excited by a plane P wave. The horizontal axis is dimensionless (t/T). The synthetic traces by four finite-difference schemes KBD, SGES, FD2, and FD4 are compared with those produced by an independent Aki-Larner method, AL (Fig. 5 of Bard and Bouchon, 1985). The vertical component is presented.

order and fourth-order computations, choosing it close to $k_M = h/(1.65 \alpha_{max})$, and α_{max} standing for the maximum P -wave velocity in the model. This choice was motivated by the stability condition of the fourth-order P -SV scheme of Levander (1988), despite the fact that it yields k smaller than necessary for second-order schemes. In particular, $k = 0.99 k_M$ has been used in models A and C and $k = 0.96 k_M$ in model B. The computations with halved spatial (and/or time) steps were utilized for checking the convergence.

The free surface in the FD2, FD4, and SGES schemes has been treated by the vacuum formalism. This choice in the cases of the FD2 and FD4 schemes has

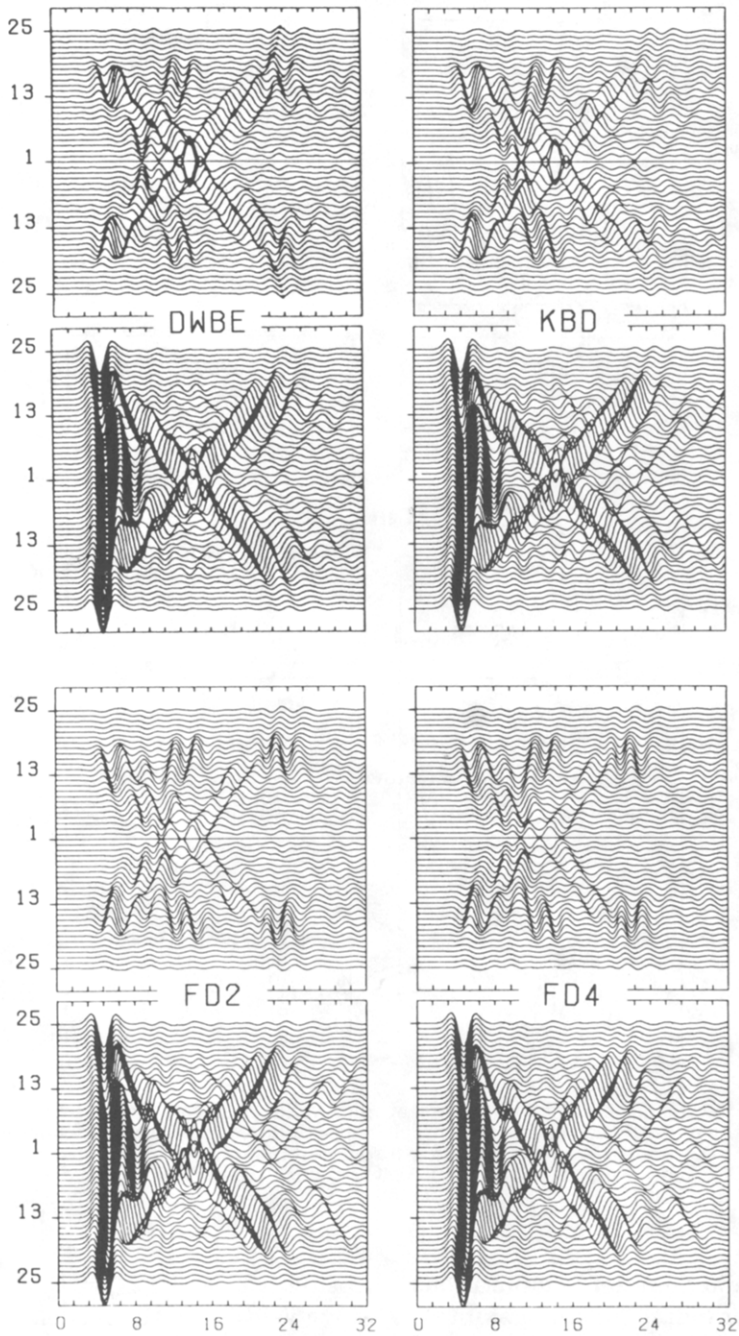


FIG. 5. Synthetic seismograms for a sedimentary basin model C, excited by a plane P wave. The horizontal axis is dimensionless (t/T). The synthetic traces by four finite-difference schemes KBD, SGES, FD2, and FD4 are compared with those produced by an independent discrete wavenumber boundary element method, DWBE (Fig. 5.17 of Kawase, 1990). Both horizontal and vertical components are presented in the *top* and the *bottom* panels, respectively. The wave field is shown for receivers 1 to 25 of Figure 2 and also for those located symmetrically with respect to receiver 1.

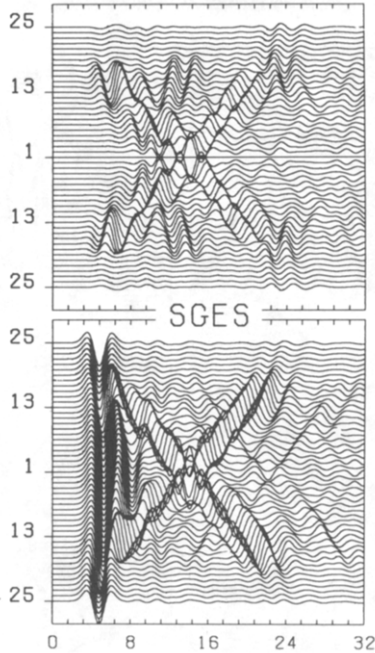


FIG. 5 (continued).

been motivated by the desire for consistency with the treatment of the internal discontinuities. As for the SGES scheme, the vacuum formalism was theoretically shown to satisfy the traction-free condition. In the case of KBD scheme, where the vacuum formalism failed in satisfying the traction-free condition, special formulas were used (see Appendix 2).

Using the SGES scheme (A12) yields no reasonable results, mainly in models B and C, where the synthetics are unlimitedly growing with increasing time. This property persists even with a drastic decrease of the time step, indicating that it is not due to violation of the stability condition. The problem remains even inside the computational region bounded from all four sides by fixed surfaces ($u = w = 0$), thereby indicating that it is not due to the vacuum formalism and/or the nonreflecting boundaries. We concluded that the scheme (A12) itself might be responsible for the unsatisfactory numerical behavior. A detailed reexamination of the derivation (paper in preparation) revealed a possible modification of the scheme, which was subsequently tested in numerical experiments. In the modified SGES scheme, the material parameters of equations (A11) and (A12), $a_{-1,-1}$, $a_{-1,1}$, $a_{1,-1}$, $a_{1,1}$, are substituted by $a_{-1/2,-1/2}$, $a_{-1/2,1/2}$, $a_{1/2,-1/2}$, $a_{1/2,1/2}$. It means that λ , μ , and $\lambda + 2\mu$ are taken midway between the displacement grid points, both in the mixed and nonmixed spatial derivatives. Although derived theoretically, the modification is very similar to the empirical stabilization found by Stephen (1988). The modification does not change major theoretical results of the preceding section. The only exception is the case of Figure 1f, where the modified scheme is treating the point (0,0) as being located in the homogeneous medium. Most strongly affected by the modification are the grid points located in the vicinity of the horizontal and/or oblique discontinuity, not the grid points situated just on

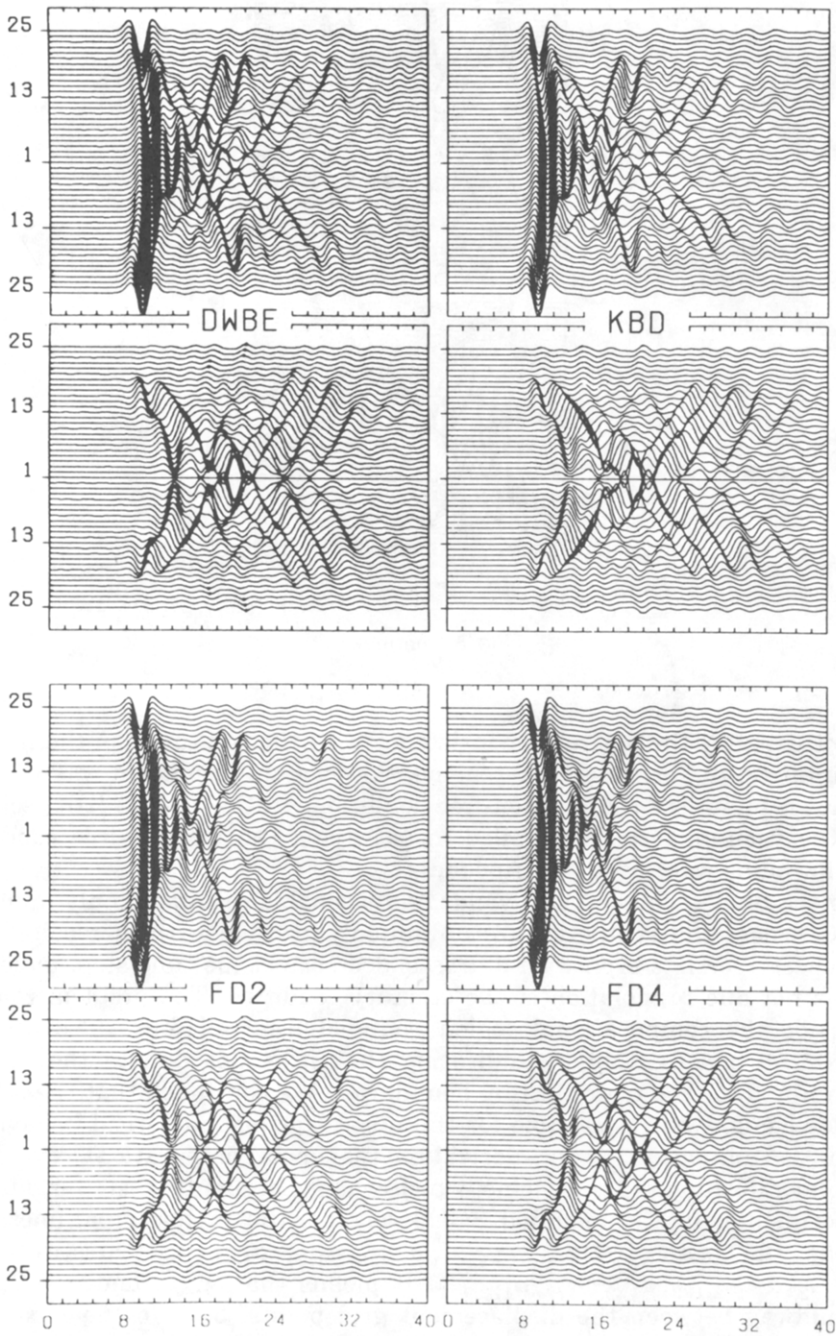


FIG. 6. Synthetic seismograms for a sedimentary basin model C, excited by a plane SV wave. The horizontal axis is dimensionless (t/T). The synthetic traces by four finite-difference schemes KBD, SGES, FD2, and FD4 are compared with those produced by an independent discrete wavenumber boundary element method, DWBE (Fig. 11 of Kawase and Aki, 1989). Both horizontal and vertical components are presented in the *top* and the *bottom* panels, respectively. The wave field is shown for the receivers 1 to 25 of Figure 2 and also for those located symmetrically with respect to receiver 1.

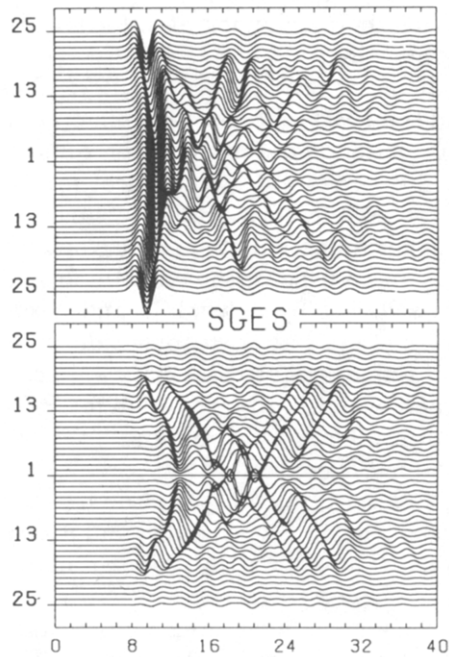


FIG. 6 (continued).

these discontinuities. What is hereafter denoted SGES means the modified SGES scheme, not that of (A12).

As it is seen from Figures 3 to 6, the individual schemes provide quite similar results. A closer examination reveals some differences increasing from model A to B and further from B to C. The results by different schemes differ mainly in their grid-dispersion properties. For example, we note that the phase velocities increase from KBD to FD2 roughly by 2% and from KBD to FD4 roughly by 4%. The increasing phase velocities are accompanied by the decreased amplitudes of later arrivals (when compared to KBD), mainly in model C.

Finally, we compare the results by finite-difference schemes with those produced by independent methods. Model A, motivated by Daley and Hron (1987), has been solved by the semianalytic method of Alekseev and Mikhailenko (1980), AM. Synthetic seismograms for models B and C were taken from the literature. In particular, model B was solved with the help of Aki-Larner discrete wavenumber method, AL, by Bard and Bouchon (1985). The discrete wavenumber boundary element method DWBE, known to be more accurate at steeply sloping discontinuities, was used in model C by Kawase and Aki (1989). All important features of the independent solutions are satisfactorily well reproduced by our synthetics in Figures 3 to 6. They include (1) the nonzero vertical components of the *PS* conversions at the normal and near normal free surface reflection in model A, (2) the bidimensional resonance in model B, and (3) the local Rayleigh waves in model C. Perhaps the most remarkable is that a very good agreement among the SGES, KBD, and DWBE results in model C.

CONCLUSIONS

1. Three recent second-order and one fourth-order finite-difference schemes for elastic waves in 2-D inhomogeneous media were theoretically investigated

and compared in terms of their behavior at internal discontinuities and free surfaces. We found the following:

(a) Both the SGES scheme of Sochacki *et al.* (1991), based on the integrated equations of motion, and the KBD scheme of Kummer *et al.* (1987), based on the differential equations of motion, were found to be consistent with the traction continuity condition at the horizontal and vertical internal discontinuities for both *SH* and *P-SV* waves. At the horizontal free surface the KBD scheme was supplemented by special formulas satisfying the vanishing-traction condition, while the SGES scheme can be used in the vacuum formalism.

(b) The FD2 and FD4 schemes by Zahradník and Hron (1992), based on the differential equations of motion, but with mixed derivatives approximated by means of the operator of Samarskii (1977, Chap. 4, Sec. 4.6), were found to be inconsistent with the traction continuity condition for *P-SV* waves at horizontal (or vertical) discontinuities, both internal and free. No problems in those situations were detected for *SH* waves.

(c) In contrast to the *SH* case, none of the studied schemes was found to be consistent with the traction continuity at a diagonal discontinuity in the case of *P-SV* waves. It is likely that this result has a more general validity for heterogeneous schemes at curved surfaces.

2. The importance of geometric averaging in the definition of the effective parameters (equation A4b) was shown for the case of *SH* waves at a horizontal discontinuity not coinciding with a grid line. Arithmetic averaging would lead to the violation of the traction-continuity condition.

3. Serious numerical problems were found for the SGES scheme until the material parameters of equations (A11) and (A12), $a_{-1,-1}$, $a_{-1,1}$, etc., were substituted by $a_{-1/2,-1/2}$, $a_{-1/2,1/2}$, etc., for λ , μ , and $\lambda + 2\mu$, in both the mixed and nonmixed spatial derivatives. This modification most strongly affected the grid points adjacent to the discontinuities. It suggests that in future theoretical studies of the finite-difference schemes more attention should be paid to their behavior in the vicinities of discontinuities.

4. Synthetic seismograms were computed by the finite-difference schemes for the models of a half-space, sediment-filled valley, and a sedimentary basin. After the above-mentioned modification in SGES scheme all the three second-order schemes (SGES, KBD, and FD2) provided similar results, despite the fact that FD2 theoretically fails in the traction continuity. This result is in agreement with that of Fornberg (1987), who reported numerical results better than predicted by the theory. It is also worth mentioning that Stephen (1988) demonstrated some heterogeneous schemes for liquid-solid interfaces, which, despite the fact that they allowed for no slip, produced results that were rather insensitive to this defect.

Similar results were also obtained by the fourth-order FD4 scheme. The latter was highly economical, since its seismograms, comparable to those produced by FD2, required about one fifth of the FD2 computer time only.

5. The finite-difference results were also compared with those from independent methods (AM, AL, and DWBE). We found that all main features of the wave fields in all the three studied models were displayed in our synthetics.

6. In general, some accuracy problems of the studied heterogeneous schemes for *P-SV* waves at curved discontinuities should be anticipated. However, the boundary introduced inaccuracies in synthetic seismograms can be relatively weak, e.g. comparable to those produced by other independent theoretical

methods, and often lower than the inaccuracies introduced by incomplete structural and/or focal data typically used.

Note: The synthetics of models A and C, presented in this paper, are available from the authors as ASCII files for possible comparisons with other methods.

ACKNOWLEDGMENTS

The presentation was improved by constructive suggestions of K. J. Marfurt, R. A. Stephen, and J. E. Vidale. The authors wish to thank the University of Alberta for supporting this cooperative work, including a short-term (J.Z.) and a long term (P.M.) visits. The first-named author was also supported through the IBM Academic Initiative in Czechoslovakia. The long-term financial support was provided, in part, by the NSERC Operating Grant and AMOCO Industrial Grant.

REFERENCES

- Aboudi, J. (1971). Numerical simulation of seismic sources, *Geophysics* **36**, 810–821.
- Alekseev, A. S. and B. G. Mikhailenko (1980). The solution of dynamic problems of elastic wave propagation in inhomogeneous media by a combination of partial separation of variables and finite-difference methods, *J. Geophys.* **48**, 161–172.
- Alterman, Z. and F. C. Karal (1968). Propagation of elastic waves in layered media by finite-difference methods, *Bull. Seism. Soc. Am.* **58**, 367–398.
- Bard, P.-Y. and M. Bouchon (1985). The two-dimensional resonance of sediment-filled valleys, *Bull. Seism. Soc. Am.* **75**, 519–541.
- Bayliss, A., K. E. Jordan, B. J. Le Mesurier, and E. Turkel (1986). A fourth-order accurate finite-difference scheme for the computations of elastic waves, *Bull. Seism. Soc. Am.* **76**, 1115–1132.
- Boore, D. M. (1972). Finite-difference methods for seismic waves, in *Methods in Computational Physics*, B. A. Bolt (Editor), Vol. 11, Academic Press, New York, 1–37.
- Daley, P. F. and F. Hron (1987). Reflection of an incident spherical P wave on a free surface (near-vertical incidence), *Bull. Seism. Soc. Am.* **77**, 1057–1070.
- Daudt, C. R., L. W. Braile, R. L. Nowack, and C. S. Chiang (1989). A comparison of finite-difference and Fourier method calculations of synthetic seismograms, *Bull. Seism. Soc. Am.* **79**, 1210–1230.
- Emerman, S. H. and R. A. Stephen (1983). Comment on “Absorbing boundary conditions for acoustic and elastic wave equations,” by R. Clayton and B. Engquist, *Bull. Seism. Soc. Am.* **73**, 661–665.
- Fornberg, B. (1987). The pseudospectral method: Comparisons with finite differences for the elastic wave equation, *Geophysics* **52**, 483–501.
- Kawase, H. (1990). Effects of topography and subsurface irregularities on strong ground motion, Ohsaki Research Inst., Report 90-02.
- Kawase, H. and K. Aki (1989). A study on the response of a soft basin for incident *S*, *P*, and Rayleigh waves with special reference to the long duration observed in Mexico City, *Bull. Seism. Soc. Am.* **79**, 1361–1382.
- Kelly, K. R., R. W. Ward, S. Treitel, and R. M. Alford (1976). Synthetic seismograms: a finite-difference approach, *Geophysics* **41**, 2–27.
- Kummer, B. and A. Behle (1982). Second-order finite-difference modeling of *SH* wave propagation in laterally inhomogeneous media, *Bull. Seism. Soc. Am.* **72**, 793–808.
- Kummer, B., A. Behle, and F. Dorau (1987). Hybrid modeling of elastic-wave propagation in two-dimensional laterally inhomogeneous media, *Geophysics* **52**, 765–771.
- Levander, A. R. (1988). Fourth-order finite-difference *P-SV* seismograms, *Geophysics* **53**, 1425–1436.
- Moczo, P. (1989). Finite-difference technique for *SH*-waves in 2-D media using irregular grids: application to the seismic response problem, *Geophys. J. Int.* **99**, 321–329.
- Reynolds, A. C. (1978). Boundary conditions for the numerical solution of wave propagation problems, *Geophysics* **43**, 1099–1110.
- Samarskii, A. A. (1977). *Theory of Difference Schemes*, Nauka, Moscow (in Russian).
- Sochacki, J. S., J. H. George, R. E. Ewing, and S. B. Smithson (1991). Interface conditions for acoustic and elastic wave propagation, *Geophysics* **56**, 168–181.
- Sochacki, J., R. Kubichek, J. George, W. R. Fletcher, and S. Smithson (1987). Absorbing boundary conditions and surface waves, *Geophysics* **52**, 60–71.

- Stephen, R. A. (1983). A comparison of finite difference and reflectivity seismograms for marine models, *Geophys. J. R. Astr. Soc.* **72**, 39–58.
- Stephen, R. A. (1988). A review of finite difference methods for seismo-acoustics problems at the seafloor, *Rev. Geophys.* **26**, 445–458.
- Van den Berg, A. P. (1987). *A Hybrid Method for the Solution of Seismic Wave Propagation Problems* (Geologica Ultraiectina, No. 49), Utrecht University, Utrecht.
- Vidale, J. E. and R. W. Clayton (1986). A stable free-surface boundary condition for two-dimensional elastic finite-difference wave simulation, *Geophysics* **51**, 2247–2249.
- Virieux, J. (1986). *P-SV* wave propagation in heterogeneous media: velocity-stress finite-difference method, *Geophysics* **51**, 889–901.
- Zahradník, J. (1985). Programs for computing and analyzing *SH* wave fields in two-dimensional absorbing block structures, in *Programs for Interpreting Seismic Observations*, N. N. Matveeva (Editor), Vol. 3, Nauka, Lennigrad, 124–186 (in Russian).
- Zahradník, J. (1990). Accelerograms influenced by local conditions: example from Forgia-Cornino (Italy), in *Prediction of Earthquakes*, C. S. Oliveira (Editor), Vol. 1, Nat. Lab. Civil Eng., Lisbon, 535–542.
- Zahradník, J. and F. Hron (1987). Seismic ground motion of sedimentary valleys: example La Molina, Lima, Peru, *J. Geophys.* **62**, 31–37.
- Zahradník, J. and F. Hron (1992). Robust finite-difference scheme for elastic waves on coarse grids, *Studia Geoph. et Geod.* **36**, 1–19.
- Zahradník, J. and L. Urban (1984). Effect of a simple mountain range on underground seismic motion, *Geophys. J. R. Astr. Soc.* **79**, 167–183.

DEPARTMENT OF GEOPHYSICS
 FACULTY OF MATHEMATICS AND PHYSICS
 CHARLES UNIVERSITY
 V HOLEŠOVIČKÁCH 2
 180 00 PRAHA 8
 CZECHOSLOVAKIA
 (J.Z.)

DEPARTMENT OF PHYSICS
 UNIVERSITY OF ALBERTA
 EDMONTON, T6G 2J1, CANADA
 (F.H., P.M.)

Manuscript received 27 February 1992

APPENDIX 1: FINITE-DIFFERENCE SCHEMES

Let us consider a linearly elastic, nonabsorbing, isotropic medium in which x , y , and z components of the displacement vector are denoted u , v , w , and time by t . If we further introduce the Lamé parameters λ , and μ and the density ρ , the equations of motion for coupled *P-SV* waves in a 2-D model with cartesian coordinates x and z then read

$$([\lambda + 2\mu]u_x)_x + (\mu u_z)_z + (\lambda w_z)_x + (\mu w_x)_z = \rho u_{tt}, \quad (\text{A1a})$$

$$(\mu w_x)_x + ([\lambda + 2\mu]w_z)_z + (\mu u_z)_x + (\lambda u_x)_z = \rho w_{tt}, \quad (\text{A1b})$$

while for the independent *SH* waves we have

$$(\mu v_x)_x + (\mu v_z)_z = \rho v_{tt}. \quad (\text{A1c})$$

We will solve equations (A1a to c) with the help of three second-order schemes adopted (with modifications) from Kummer *et al.* (1987), Sochacki *et al.* (1991), and Zahradník and Hron (1992). For simplicity, a uniform square grid of space step h and time step k is employed in all the studied schemes. Since the temporal derivatives are approximated by the same second-order central differences in all three schemes, we will concentrate only on the nonmixed and mixed spatial derivatives, whose prototypes will be denoted $(af_z)_z$, $(af_x)_z$.

KBS Scheme (after Kummer et al., 1987)

The nonmixed derivative is approximated by the well-known method of Tikhonov and Samarskii (e.g., Samarskii, 1977, Chap. 4, Sec. 4.6; Boore, 1972). Following this method function g is introduced by $af_z = g$ and the derivative $(af_z)_z = g_z$ is approximated by the central difference (Fig. A1a).

$$g_z \doteq (g_{0,1/2} - g_{0,-1/2})/h. \tag{A2}$$

When expressing $g_{0,1/2}$, the equation $g/a = f_z$ is integrated between the grid points $(0, 0)$, $(0, 1)$, and the mean-value theorem is employed:

$$g_{0,1/2} \int_{0,0}^{0,1} dr/a \doteq \int_{0,0}^{0,1} f_z dz = f_{0,1} - f_{0,0}. \tag{A3}$$

The approximation of $g_{0,-1/2}$ is analogous, leading to

$$(af_z)_z \doteq 1/h^2 \{ a_H (f_{0,1} - f_{0,0}) - a_G (f_{0,0} - f_{0,-1}) \}, \tag{A4a}$$

$$a_G = h \left[\int_{0,-1}^{0,0} dz/a \right]^{-1}, \quad a_H = h \left[\int_{0,0}^{0,1} dz/a \right]^{-1}, \tag{A4b}$$

where two effective parameters a_G and a_H are geometric averages (sometimes

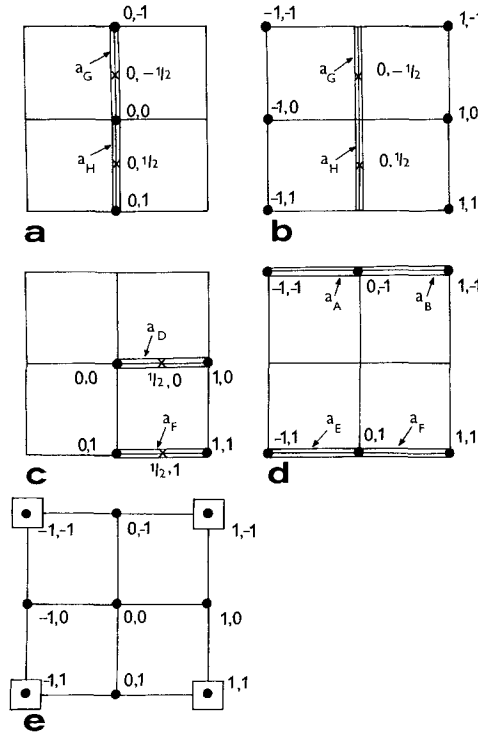


FIG. A1. Schematic representation of the approximations used for spatial derivatives in the analyzed finite-difference schemes. The grid points employed for the *displacement* approximations are marked by full circles. Auxiliary displacement approximations, used in the derivation only, are shown by crosses. Rectangles and small squares denote the *effective and local parameters of the medium*, respectively.

also called harmonic averages) of the material parameter a over two vertical grid legs (Fig. A1a). The mixed derivative $(af_x)_z$ is more complicated. The outer derivative is again approximated by (A2). For expressing $g_{0,1/2}$ we now get

$$g_{0,1/2} \int_{0,0}^{0,1} dr/a \doteq \int_{0,0}^{0,1} f_x dz. \quad (\text{A5a})$$

The integration on the right-hand side is this time over z , hence the derivative f_x is to be expressed as a function of z . The Taylor expansion was proposed for this purpose by Kummer *et al.* (1987). Function f must be expanded to the third order if the second-order accuracy of g_z is to be achieved. After substitution of the corresponding expansion into (A5a), integration of the right-hand side, and introduction of a_H according to (A4b), we get

$$g_{0,1/2} \doteq a_H(f_x + hf_{xz}/2 + h^2f_{xzz}/6). \quad (\text{A5b})$$

The three derivatives f_x , f_{xz} , and f_{xzz} are approximated by standard finite-difference formulas:

$$\begin{aligned} f_x &\doteq (f_{1,0} - f_{-1,0})/2h, \\ f_{xz} &\doteq (f_{1,1} - f_{1,-1} - f_{-1,1} + f_{-1,-1})/4h^2, \\ f_{xzz} &\doteq (f_{1,1} - f_{-1,1} - 2[f_{1,0} - f_{-1,0}] + f_{1,-1} - f_{-1,-1})/2h^3. \end{aligned} \quad (\text{A5c})$$

Then $g_{0,-1/2}$ is approximated in the same manner. Finally, on the grid stencil of Figure 1b, we obtain

$$\begin{aligned} (af_x)_z &\doteq 1/2h^2\{(a_H - a_G)(f_{1,0} - f_{-1,0}) \\ &\quad + 1/6(a_H - a_G)(f_{1,1} - f_{-1,1} - 2[f_{1,0} - f_{-1,0}] + f_{1,-1} - f_{-1,-1}) \\ &\quad + 1/4(a_H + a_G)(f_{1,1} - f_{1,-1} - f_{-1,1} + f_{-1,-1})\}. \end{aligned} \quad (\text{A6})$$

It is worth mentioning that the effective parameters remain the same as those for the nonmixed derivative in (A4).

FD2 Scheme (after Zahradník and Hron, 1992)

In this scheme, the nonmixed derivative is also given by (A4), and function $g = af_x$ is again introduced in the mixed derivatives. The approximation of g_z is then accomplished in two steps, following Samarskii (1977, Chap. 4, Sec. 4.6). We start with the first-order approximation (Fig. A1c):

$$g_z \doteq (g_{1/2,1} - g_{1/2,0})/h. \quad (\text{A7})$$

It allows $g_{1/2,1}$ to be expressed by integrating f_x with respect to x , not z :

$$g_{1/2,1} \int_{0,1}^{1,1} dx/a \doteq \int_{0,1}^{1,1} f_x dx = f_{1,1} - f_{0,1}, \quad (\text{A8a})$$

$$g_{1/2,1} \doteq a_F(f_{1,1} - f_{0,1})/h, \quad (\text{A8b})$$

with a_F being an effective parameter. The treatment of $g_{1/2,0}$ is analogous and

a_D is introduced. The second-order accuracy is achieved by repeating this step four times and evaluating the arithmetic average:

$$\begin{aligned} L^1 f &= 1/h^2 \{a_E(f_{0,1} - f_{-1,1}) - a_C(f_{0,0} - f_{-1,0})\}, \\ L^2 f &= 1/h^2 \{a_D(f_{1,0} - f_{0,0}) - a_B(f_{1,-1} - f_{0,-1})\}, \\ L^3 f &= 1/h^2 \{a_C(f_{0,0} - f_{-1,0}) - a_A(f_{0,-1} - f_{-1,-1})\}, \\ L^4 f &= 1/h^2 \{a_F(f_{1,1} - f_{0,1}) - a_D(f_{1,0} - f_{0,0})\}, \\ (af_x)_z &\doteq 1/4(L^1 + L^2 + L^3 + L^4)f. \end{aligned} \tag{A9}$$

After cancellation of some terms, only six points and four effective parameters remain in the resulting formula (see Fig. A1d):

$$\begin{aligned} (af_x)_z &\doteq 1/4(L^1 + L^2 + L^3 + L^4)f \\ &= 1/4h^2 [a_A f_{-1,-1} - (a_A - a_B)f_{0,-1} - a_B f_{1,-1} \\ &\quad - a_E f_{-1,1} - (a_F - a_E)f_{0,1} + a_F f_{1,1}]. \end{aligned} \tag{A10}$$

A higher number of the effective parameters appear in (A10) than in (A6). This feature indicates an increased dependence of the scheme (A10) on the spatial variations of the material parameters in smoothly varying media, but it does not necessarily guarantee a better behavior at discontinuities.

The fourth-order version of the same scheme, called FD4, was also developed by Zahradník and Hron (1992). It makes use of the formula (A10) and an analogous formula with a doubled step $2h$, whose linear combination with weights $\frac{4}{3}$ and $-\frac{1}{3}$ yields the fourth-order accuracy.

SEGS Scheme (after Sochacki et al., 1991)

In this method, the spatial derivatives are approximated by a technique that is fundamentally different from those employed in the KBD and FD2 schemes. In constructing the SEGS scheme, the equations of motion (A1) are integrated over a grid cell, the divergence theorem is applied, and, wherever the grid cell is crossed by the material discontinuity, the traction-continuity condition is applied. Finally, the integral over the surface of the grid cell is discretized with the second-order accuracy. The SEGS scheme is given by formula (28) in their paper.

It can be easily found that the nonmixed derivative of the SEGS scheme is expressed similarly to that in equation (A4a). The only difference is that the local parameter values, rather than the effective parameters, are used in the SEGS scheme:

$$a_G \rightarrow 1/2(a_{-1,-1} + a_{1,-1}), \quad a_H \rightarrow 1/2(a_{-1,1} + a_{1,1}). \tag{A11}$$

The mixed derivative in the SEGS scheme (see Fig. A1e) reads

$$\begin{aligned} (af_x)_z &\doteq 1/4h^2 \{a_{-1,1}(f_{0,1} - f_{-1,1}) - a_{-1,-1}(f_{0,0} - f_{-1,0}) \\ &\quad + a_{1,1}(f_{1,0} - f_{0,0}) - a_{1,-1}(f_{1,-1} - f_{0,-1}) \\ &\quad + a_{-1,1}(f_{0,0} - f_{-1,0}) - a_{-1,-1}(f_{0,-1} - f_{-1,-1}) \\ &\quad + a_{1,1}(f_{1,1} - f_{0,1}) - a_{1,-1}(f_{1,0} - f_{0,0})\}. \end{aligned} \tag{A12}$$

Equation (A12) is significantly different from (A6), but (rather surprisingly)

similar to (A10). The similarity becomes evident when an equivalent form of (A10) is used, viz. (A9). The only difference is in the approximation of the material parameter, a . The FD2 scheme can be transformed into the SGES scheme by substituting

$$\begin{aligned} a_A &\rightarrow a_{-1,-1}, & a_B &\rightarrow a_{1,-1}, & a_E &\rightarrow a_{-1,1}, & a_F &\rightarrow a_{1,1}, \\ a_C &\rightarrow a_{-1,-1} \text{ in } L^1, & \text{and } a_C &\rightarrow a_{-1,1} \text{ in } L^3, \\ a_D &\rightarrow a_{1,1} \text{ in } L^2, & \text{and } a_D &\rightarrow a_{1,-1} \text{ in } L^4. \end{aligned} \quad (\text{A13})$$

In other words, the SGES scheme can be also obtained through extending the FD2 scheme by an additional term,

$$1/4h^2\{(a_E - a_A)(f_{0,0} - f_{-1,0}) + (a_F - a_B)(f_{1,0} - f_{0,0})\}. \quad (\text{A14})$$

Naturally, a similar term is added in case of $(af_z)_x$.

APPENDIX 2. FREE-SURFACE FORMULAS

The finite-difference formulas of Kummer *et al.* (1987), referred to as the KBD scheme in the main text and Appendix 1, apply to internal grid points. Their extension, which is applicable to a flat free surface and consistent with the vanishing-traction condition, is derived here. Hereafter, the grid stencil of Figure A1c is used with point $(0, 0)$ being now the free-surface point.

The derivative $(af_x)_x$ remains the same as for the internal points. The derivative $(af_z)_z$ is approximated as follows:

$$\begin{aligned} af_z &= g, \\ g_z &\doteq 2(g_{0,1/2} - g_{0,0})/h, \end{aligned}$$

where

$$\begin{aligned} g_{0,0} &\doteq a_{0,0}(f_{0,1} - f_{0,0})/h, \\ g_{0,1/2} &\doteq a_H(f_{0,1} - f_{0,0})/h. \end{aligned}$$

Here a_H is the effective parameter, defined in equation (A4b) of Appendix 1 as an integral average along a grid leg, whereas $a_{0,0}$ is a local approximation to the material parameter a at point $(0, 0)$. Finally,

$$(af_z)_z \doteq 2(a_H - a_{0,0})(f_{0,1} - f_{0,0})/h^2.$$

The derivative $(af_x)_z$ is approximated as

$$\begin{aligned} af_x &= g, \\ g_z &\doteq 2(g_{0,1/2} - g_{0,0})/h, \end{aligned}$$

where

$$\begin{aligned} g_{0,0} &\doteq a_{0,0}(f_{1,0} - f_{-1,0})/2h, \\ g_{0,1/2} &\doteq a_H(f_x + hf_{xz}/2 + h^2f_{xzz}/6). \end{aligned}$$

The latter formula $(g_{0,1/2})$ is the same as for the internal gridpoints, but f_{xz}

and f_{xzz} are now treated in a different manner:

$$f_{xz} \doteq (f_{1,1} - f_{1,0} - f_{-1,1} + f_{-1,0})/2h^2,$$

$$f_{xzz} \doteq (f_{1,1} - f_{1,0} - f_{-1,1} + f_{-1,0})/h^3 - 2f_{xz}/h.$$

Finally,

$$(af_x)_z \doteq (1/2h^2)\{(a_H - 2a_{0,0})(f_{1,0} - f_{-1,0}) + a_H(f_{1,1} - f_{-1,1})\}.$$

The derivative $(af_z)_x$ is treated as in the case of the internal points except the approximations of f_z , f_{zx} , and f_{zxx} , for which we now take

$$f_z \doteq (f_{0,1} - f_{0,0})/h,$$

$$f_{zx} \doteq (f_{1,1} - f_{1,0} - f_{-1,1} + f_{-1,0})/2h^2,$$

$$f_{zxx} \doteq (f_{1,1} - f_{1,0} - 2[f_{0,1} - f_{0,0}] + f_{-1,1} - f_{-1,0})/h^3.$$

Finally,

$$(af_z)_x \doteq 1/h^2\{1/6(a_D - a_C)[f_{1,1} - f_{1,0} + 4(f_{0,1} - f_{0,0}) + f_{-1,1} - f_{-1,0}]$$

$$+ 1/4(a_D + a_C)[f_{1,1} - f_{1,0} - f_{-1,1} + f_{-1,0}]\}.$$

Here a_D is the effective parameter between points 0, 0 and 1, 0 analogous to a_D of Figure A1c in Appendix 1. Likewise, a_C refers to the leg between the grid points -1, 0 and 0, 0.